

Constraints on the Sunyaev-Zel’dovich signal from the Warm Hot Intergalactic Medium from WMAP and SPT data

Ricardo Génova-Santos,^{1,2*} I. Suarez-Velásquez,³ F. Atrio-Barandela,⁴
and J. P. Mücke³

¹ *Instituto de Astrofísica de Canarias, 38200 La Laguna, Tenerife, Canary Islands, Spain*

² *Departamento de Astrofísica, Universidad de La Laguna (ULL), 38206 La Laguna, Tenerife, Spain*

³ *Leibniz Institut für Astrophysik, 14482 Potsdam, Germany*

⁴ *Física Teórica, Universidad de Salamanca, 37008 Salamanca, Spain*

Accepted Received In original form

ABSTRACT

The fraction of ionized gas in the Warm Hot Intergalactic Medium induces temperature anisotropies on the Cosmic Microwave Background similar to those of clusters of galaxies. The Sunyaev-Zel’dovich anisotropies due to these low density, weakly non-linear, baryon filaments can not be distinguished from that of clusters using frequency information, but they can be separated since their angular scales are very different. To determine the relative contribution of the WHIM SZ signal to the radiation power spectrum of temperature anisotropies, we explore the parameter space of the concordance Λ -Cold Dark Matter model using Monte Carlo Markov Chains and the Wilkinson Microwave Anisotropy Probe 7yr and South Pole Telescope data. We find marginal evidence of a contribution by diffuse gas, with amplitudes of $A_{\text{WHIM}} = 10 - 20 \mu\text{K}^2$, but the results are also compatible with a null contribution from the WHIM, allowing to set an upper limit of $A_{\text{WHIM}} < 43 \mu\text{K}^2$ (95.4% C.L.). The signal produced by galaxy clusters remains at $A_{\text{CL}} = 4.5 \mu\text{K}^2$, a value similar to what is obtained when no WHIM is included. From the measured WHIM amplitude we constrain the temperature-density phase diagram of the diffuse gas, and find it to be compatible with numerical simulations. The corresponding baryon fraction in the WHIM varies from 0.43 to 0.47, depending on model parameters. The forthcoming Planck data could set tighter constraints on the temperature-density relation.

Key words: Cosmology: cosmic microwave background - cosmological parameters; Cosmology - theory; Cosmology - observations

1 INTRODUCTION

At low redshifts, close to half of the baryons in the Universe have yet to be identified (Fukugita & Peebles, 2004). Numerical simulations suggest the existence of a Warm-Hot Intergalactic Medium (WHIM) phase of mildly non-linear structures (Cen & Ostriker, 1999, 2006; Davé et al. 2004; Smith et al. 2011; Shull, Smith & Danforth, 2012). Most of the efforts

to detect the WHIM has concentrated in the identification of X-ray absorbers, and around half of the WHIM baryons could have been identified through this method, leaving the remaining missing baryon fraction at $\sim 29 \pm 13\%$ (Shull et al. 2012). However, many of these detections at $z > 0$ are either of low statistical significance or controversial. For instance, the X-ray detections by Nicastro et al. (2005) have not been confirmed by later studies (Kaastra et al. 2006, Yao et al. 2012). As an observational alternative, Atrio-Barandela & Mücke (2006) suggested that the WHIM could

* E-mail: rgs@iac.es

be detected through the temperature anisotropies generated on the Cosmic Microwave Background (CMB). Due to thermal and kinetic motions of ionized gas, Compton scattering of CMB photons by free electrons induces secondary temperature anisotropies that were first described by Sunyaev & Zeldovich (1970, 1972, hereafter SZ, Birkinshaw, 1999). The thermal SZ (TSZ) temperature anisotropies have a distinctive frequency dependence, different from other foregrounds, and have been detected in the direction of many known clusters (see e.g. Planck Collaboration, 2011). The detection of the TSZ signal associated with the less-dense WHIM inter-cluster filaments is rather more challenging owing to its small amplitude. Hernández-Monteagudo, Génova-Santos & Atrio-Barandela (2004) attempted to measure this signal through cross-correlations between CMB maps and templates of the density field constructed from galaxy catalogues (see also Suarez-Velásquez et al. 2013a). Génova-Santos et al. (2008) detected a temperature decrement towards the Corona Borealis supercluster, in a position with no known clusters but with an overpopulation of galaxies (Padilla-Torres et al. 2009), but could not confirm it was associated to WHIM gas. More recently, an unambiguous measurement of a hot and diffuse gas component outside the virial regions of clusters was obtained by combining X-ray and CMB data from the ROSAT and Planck satellites on the cluster pair A399-A401 (Planck Collaboration, 2012). The other SZ component, the KSZ effect, is more difficult to detect even towards galaxy clusters since it has the same frequency dependence as the intrinsic CMB signal. Only the average KSZ effect due to large samples of clusters (Kashlinsky et al. 2008, 2010) or galaxies (Hand et al. 2012) has been detected.

Frequency information can not be used to distinguish the TSZ anisotropy due to clusters and WHIM filaments, but they could be separated using the different scale of their respective anisotropies. The cluster TSZ contribution is maximum at $\ell_{max} \sim 3000$ (Atrio-Barandela & Mückel, 1999) while the thermal and kinematic SZ due to the WHIM is in the range $\ell_{max} \simeq 200 - 500$, depending on model parameters (Atrio-Barandela & Mückel 2006, Atrio-Barandela, Mückel & Génova-Santos 2008, Suarez-Velásquez, Mückel & Atrio-Barandela 2013b). To successfully separate the WHIM from the cluster SZ contribution, the latter needs to be well characterized. The analysis of the Wilkinson Microwave Anisotropy Probe (WMAP) 7 year data confirmed that the SZ power spectrum due to the unresolved cluster population was a factor 0.45 ± 0.06 the theoretical predictions and estimates based on numerical simulations (Komatsu et al 2011). This lower than expected amplitude agreed with the independent results from the South Pole Telescope (SPT, Keisler et al 2011), suggesting that the current models of the intracluster medium overestimates the gas pressure relative to X-ray and CMB observations (Komatsu et al. 2011). An alternative explanation relies on the fact that the TSZ power spectrum depends on the amplitude of the matter density fluctuations, σ_8 , as $C_\ell^{CL} \propto (\sigma_8)^7$ (Komatsu & Kitayama 1999). If the measured value $\sigma_8 = 0.801 \pm 0.030$

(Larson et al. 2011) were overestimated, so it would be the theoretical prediction for the TSZ amplitude. A lower σ_8 would also result in a lower amplitude of the primordial CMB anisotropies at low ℓ , which then could accommodate a WHIM component to compensate for this power deficit. In Génova-Santos (2009) we showed that a 2-3% variation of the concordance Λ CDM model value of σ_8 allowed a contribution of the WHIM of amplitude $\ell(\ell+1)C_\ell/2\pi \simeq 100 \mu\text{K}^2$ at $\ell \sim 200$.

In the present paper we first analyze the combined WMAP 7yr and SPT data, the best available data set to date, constraining the power spectrum out to $\ell = 3000$, in order to search for any WHIM SZ contribution to the CMB radiation power spectrum. Due to the difference in scale, the WHIM and cluster anisotropies can be separated through their power spectrum. Since WMAP probes scales below $\ell \leq 1000$ it is mostly sensitive to the WHIM. SPT data, that probes $\ell \geq 600$, can constrain better the cluster component. By combining both data sets, we could separate both contributions to TSZ anisotropies. Second, we study if the WHIM component brings the cluster contribution in agreement with the theoretical and numerical expectations. In Sec. 2 we describe the WHIM model and its parameters; in Sec. 3 we describe the power spectrum analysis implemented in Monte Carlo Markov Chains (MCMC); in Sec. 4 we discuss our main results and in Sec. 5 we summarize our conclusions.

2 TEMPERATURE ANISOTROPIES GENERATED BY THE WARM HOT INTERGALACTIC MEDIUM

In our model, we define the WHIM as shock-heated intergalactic gas at density contrasts in the range $\delta_B = [1, 100]$ and temperatures $10^5\text{K} < T < 10^7\text{K}$. We take a rather low upper limit for δ_B in order to clearly distinguish the WHIM in the less dense inter-cluster filaments that form the cosmic web from the gas surrounding clusters of galaxies. The WHIM phase of our model encompasses the fraction of the missing baryons with $\delta_B \leq 100$. Due to the low upper limit of δ_B chosen by us, the contributions of the WHIM to the CMB anisotropy spectrum in our model must be considered as a lower limit to the true anisotropy.

To compute the TSZ power spectrum of this WHIM phase, we assume that at any given point the probability of having a filament with a baryon density contrast $\delta_B > 1$ is given by the log-normal probability density function (PDF, Atrio-Barandela & Mückel 2006). The log-normal PDF was introduced by Coles & Jones (1991) to describe the non-linear distribution of matter in the Universe. It has been applied to the column density distribution for neutral hydrogen in the intergalactic medium (Choudhury et al. 2001) and it has been found to describe very well the matter statistics at scales larger than $7h^{-1}\text{Mpc}$ (Kitaura et al. 2009). In the log-normal model, the power spectrum of the baryon density inhomogeneities follows the dark matter distribu-

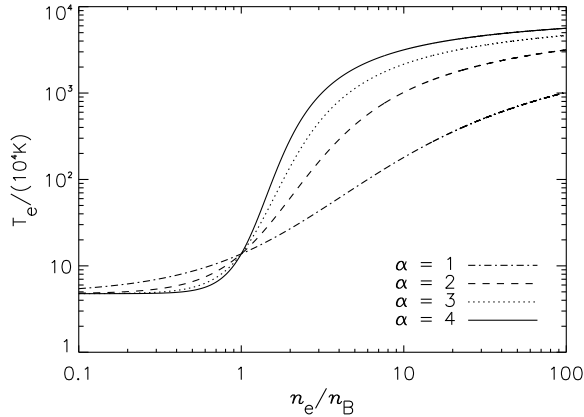


Figure 1. Different fits of the phase diagram of the hydrodynamical simulations of Kang et al (2005). From bottom to top the dotted, dashed, dot-dashed and solid lines correspond to values 1,2,3 and 4 of the α parameter given in eq. (1).

tion above a linear scale L_0 . Below this cut-off scale, baryon density perturbations are smoothed out due to physical effects like Jeans dissipation or shock heating. At the physical conditions present in the WHIM, shock heating is the dominating process and $L_0(z)$ is the scale at which the linear peculiar velocity $v_p(\mathbf{x}, \mathbf{z})$ is equal or larger than the sound speed $c_s(z)$ of the baryon fluid at redshift z (for details, see Suarez-Velásquez et al. 2013b). The sound speed is given by the mean temperature of the Intergalactic Medium (IGM) as $c_s = (k_B T_{\text{IGM}}(z)/m_p)^{1/2}$, where m_p is the proton mass. At every redshift, the IGM temperature varies with location, but the average value, T_{IGM} , determines the smallest baryon density perturbation that survives shock heating. The evolution of the IGM temperature is mostly determined by the UV background. The mean IGM temperature variation with redshift is small and we approximate it by $\log_{10}(T_{\text{IGM}}/10^3 \text{K}) = (A+0.1(1+z))$ (Theuns et al. 2002). At redshifts $z \leq 3$ the temperature varies in the range $T_{\text{IGM}} = 10^{3.6} - 10^{4.0}$ K (Tittley & Meiksin, 2007); consequently, $A = 0.5 - 0.9$. At redshifts $z > 3$ the WHIM does not generate significant temperature anisotropies and its contribution can be ignored. When T_{IGM} increases, more baryon fluctuations are erased and the size of baryon filaments increases, subtending a larger angle and giving rise to CMB temperature anisotropies at larger angular scales. The corresponding scale at $z = 0$ is $L_0 \simeq 1.7(T_{\text{IGM}}/10^{4.0} \text{K})^{1/2} h^{-1} \text{Mpc}$.

To compute the TSZ temperature anisotropies, it is necessary to determine the number of free electrons in each filament and their average temperature. The number density of electrons n_e can be obtained by assuming equilibrium between ionization (collisional and photo-ionization) and recombination. At temperatures $T = 10^5 - 10^7$ K and density contrasts $\delta_B \leq 100$, the gas can be considered fully ionized. Whereas in Atrio-Barandela & Mücke (2006) we used a polytropic equation of state, in Suarez-Velásquez et

al. (2013b) we used fits of the phase diagrams obtained in various hydrodynamical simulations to take into account the effect of shock heating in the evolution of the WHIM. We used

$$\log_{10} \left(\frac{T_e(\xi)}{10^8 \text{K}} \right) = - \frac{2}{\log_{10}(4 + \xi^{\alpha+1/\xi})}, \quad (1)$$

since this numerical fit reproduces well the phase diagram of Kang et al. (2005). In this expression, $\xi = n_e/\bar{n}_B \simeq \delta_B + 1$ is the electron density in units of the mean baryon density. The phase diagrams derived from the simulations are not simple linear relations of the type $T = T(\xi)$, but have a large scatter. The α parameter of the previous equation is introduced to model this uncertainty. We consider an interval wide enough, from $\alpha = 1$ to $\alpha = 4$, in order to properly cover all the possible variations found in the simulations. In Fig. 1 we represent the resulting equations of state for $\alpha = (1, 2, 3, 4)$ in decreasing order from top to bottom.

In our model, the correlation function of the spatial variations of the electron pressure along two lines of sight separated by an angle θ is

$$C(\theta) = \int_0^{z_f} \int_0^{z_f} \langle S(\hat{x}_1, z_1) S(\hat{x}_2, z_2) \rangle dz_1 dz_2. \quad (2)$$

In this expression $S = G(\nu)(k_B \sigma_T/m_e c^2) n_e T_e (dl_i/dz_i)$ with $i = (1, 2)$. Integrations are carried out along the line of sight l . For each direction, the TSZ WHIM temperature anisotropy is $\Delta T = y_c G(\nu)$, with $y_c = k_B \sigma_T/m_e c^2 \int T_e n_e dl$ the integrated Comptonization parameter, n_e the electron density, T_e the electron temperature, $m_e c^2$ the electron annihilation temperature, k_B the Boltzmann constant, σ_T Thomson cross section, dl the line element, dz its corresponding redshift interval and $G(\nu) = (x \coth(x/2) - 4)$ the frequency dependence of the TSZ effect with $x = h\nu/kT_0$ the reduced frequency and T_0 the CMB temperature. Expanding eq. (2) in Legendre polynomials gives the WHIM contribution to the power spectrum of CMB temperature anisotropies

$$C_\ell = 2\pi \int_{-1}^{+1} C(\theta) P_\ell(\cos \theta) d \cos \theta \quad (3)$$

where P_ℓ is the Legendre polynomial of multipole ℓ .

The radiation power spectrum depends on the underlying cosmological model and the parameters describing the physical state of the WHIM, as shown in Fig. 2. The Λ CDM cosmological parameters have been fixed to the best fit values of WMAP 7yr data. In Fig. 2a we represent the spectra for different fits of the equation of state. The IGM temperature, that parametrizes the cut-off length of the baryon power spectrum L_0 , is $T_{\text{IGM}} = 10^{3.6}$ K, while the amplitude of matter fluctuations is $\sigma_8 = 0.7$. From bottom to top the fit parameter of the equation of state is $\alpha = 1, 2, 3, 4$. At densities $\xi \geq 2$ the temperature of the free electrons in the WHIM increases with increasing α and the resulting temperature anisotropies also increase. The filled circles show the position of the maxima, that in this case vary in the range $\ell =_{\text{max}} [270, 350]$. The variation is smaller for larger σ_8 . These maxima correspond to angular scales in the range

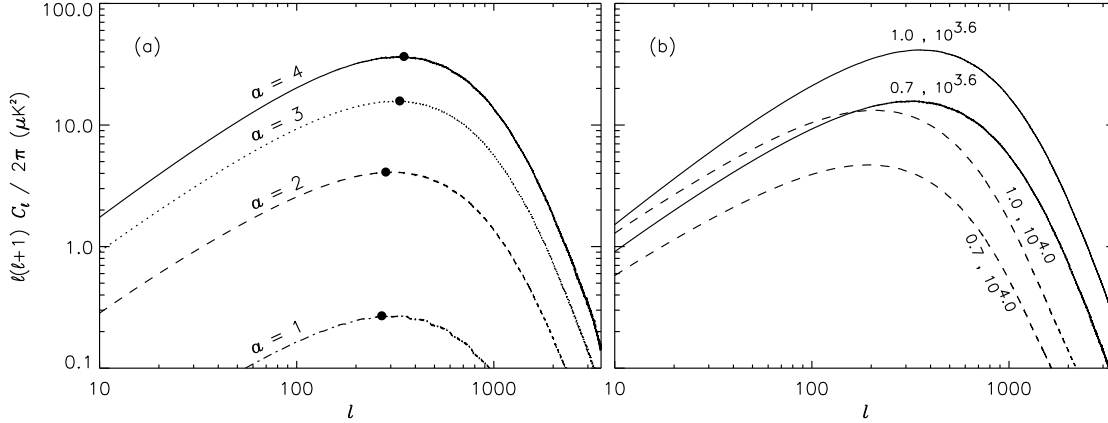


Figure 2. Radiation power spectra for different WHIM model parameters. (a) Variation with the α parameter given in eq. 1. From bottom to top the dot-dashed, dashed, dotted and solid lines correspond respectively to $\alpha = 1, 2, 3, 4$, with $T_{\text{IGM}} = 10^{3.6}$ K and $\sigma_8 = 0.7$. All other parameters are fixed to the values of the concordance Λ CDM model. The maxima, indicated by filled circles, are in the range $\ell = [270, 350]$. (b) Variation with the IGM temperature and σ_8 for $\alpha = 3$. Solid and dashed lines correspond to $T_{\text{IGM}} = 10^{3.6}, 10^{4.0}$ K; for each pair, the top and bottom lines correspond to $\sigma_8 = 0.7, 1.0$, respectively.

$\simeq 40 - 50$ arcmin, much larger than ~ 7 arcmin, the scale of the power spectrum of the unresolved 0.5-2 keV Cosmic X-ray Background due to both clusters and diffuse gas (Roncarelli et al. 2012, Cappelluti et al. 2012). The difference in scale between the power spectrum of TSZ anisotropies due to clusters and due to the WHIM is not in contradiction with our result. The X-ray power spectra includes the contribution of diffuse gas from denser environments ($\delta \lesssim 10^3$); excluding those high dense regions shifts the power of the WHIM anisotropies scales larger than those of clusters. Further, since the TSZ distortion is proportional to the electron pressure, $n_e T_e$ while X-ray emissivity is proportional to $n_e^2 T_e^{1/2}$ (Birkinshaw 1999), the TSZ anisotropy will be more extended than the X-ray emission of the WHIM, as it occurs with clusters (Atrio-Barandela et al 2008).

In Fig. 2b we represent the variation with T_{IGM} and σ_8 . The solid and dashed lines correspond to $T_{\text{IGM}} = 10^{3.6}, 10^{4.0}$ K, respectively. For each pair, the top and bottom lines correspond to $\sigma_8 = 1.0$ and 0.7. The fit parameter of the equation of state is fixed at $\alpha = 3$. This figure shows that the TSZ WHIM temperature anisotropies grow with increasing σ_8 and decreasing T_{IGM} . Lowering the cut-off length results in larger anisotropies since more baryon density perturbations at small scales survive shock heating. As a result, the average angular size of baryon filaments decreases and the power spectrum is shifted to small angular scales.

3 MARKOV CHAIN MONTE CARLO ANALYSIS OF WMAP AND SPT

The shape of the SZ power spectrum, $\ell(\ell+1)C_\ell/2\pi$, is very similar for both clusters and the WHIM; it presents a single maximum at ℓ_{max} , determined by the average angular size of clusters and baryon filaments. The main difference is the

location of their maxima. As indicated in the introduction, it is this difference on angular scale that can be used to separate the contribution of the WHIM from that of clusters. In both cases, the overall shape of the spectrum is very weakly dependent on other model parameters. For instance, due to the uncertainties on the number density and pressure profile and on their scaling with cluster mass and redshift, Keisler et al. (2011) used a fixed spectral shape, derived from numerical simulations that contains both the TSZ and KSZ components, and fit its amplitude to the data. If the radiation power spectrum is written as $C_\ell^{\text{SZ}} = A_{\text{SZ}} G(\nu)^2 f(\ell)$, then $f(\ell)$ is kept constant and only A_{SZ} is derived from the data. To search for any WHIM SZ component in addition to the SZ due to clusters we will explore the parameter space of the standard Λ CDM model by fitting the theoretically predicted radiation power spectra to WMAP and SPT data including WHIM and cluster contributions. We use the COSMOMC package (Lewis & Bridle 2002), which implements a MCMC method that performs parameter estimation using a Bayesian approach. We modified the Keisler et al. (2011)¹ version by adding at each step of the chain the precomputed WHIM SZ component to the theoretical power spectrum computed with CAMB (Lewis et al. 2000).

We constructed a three-dimensional grid of WHIM models for values of $\sigma_8 = 0.7$ and 1.0, $\alpha = 1, 2, 3, 4$ and $\log(T_{\text{IGM}}/10^3 \text{K}) = A + 0.1$ with $A = [0.3, 1.1]$ varying in units of 0.1. Firstly, the power spectra for any given value of these parameters were interpolated between the pre-computed spectra corresponding to the nearest adjacent values. The interpolation was linear in A and logarithmic in α, σ_8 . For the latter, the spectra scales as $C_\ell^{\text{WHIM}} \propto$

¹ Likelihood code downloaded from <http://pole.uchicago.edu/public/data/keisler11/#Likelihood>

$\sigma_8^{2.6}(\Omega_B h)^2$ (Suarez-Velásquez et al. 2013b). Even if the interpolation procedure was accurate (errors below 1%), the chains were slowly convergent and degenerate with respect to T_{IGM} . For this reason, we removed the interpolation on the temperature and fixed T_{IGM} . Fig. 2 illustrates that varying α (Fig. 2a) and σ_8 (Fig. 2b) changes the amplitude but does not significantly modify the shape of the radiation power spectrum. To see the effect of the location of the maximum in our final results, we considered two fixed WHIM power spectra with maxima located at $\ell_{\text{max}} = 330$ and 210. Neglecting the small variations due to the different values of α , this maxima correspond to $T_{\text{IGM}} = 10^{3.6}$ and $10^{4.0}$ K, respectively. Therefore, similarly as it is done for the cluster contribution, in our MCMC's we input these two spectra and fit their amplitude (A_{WHIM}) to the data.

We fit the data, through the combined WMAP and SPT likelihoods, to a concordance Λ CDM model, defined by a spatially flat Universe with cold dark matter (CDM), baryons, and a cosmological constant Λ . Following Keisler et al. (2011) we added the combined galaxy clusters TSZ+KSZ amplitude (A_{CL}) and two amplitudes associated with the contributions from Poisson ($A_{\text{PS}}^{\text{Poisson}}$) and clustered ($A_{\text{PS}}^{\text{Clustered}}$) distributed point sources in addition to the amplitude of the WHIM TSZ signal (A_{WHIM}). The WHIM and cluster power spectra were normalized to unity at $\ell = 300$ and $\ell = 3000$, respectively. Then, to take into account the frequency dependence of the TSZ effect, their amplitudes A_{WHIM} and A_{CL} were scaled to the average frequency of WMAP V and W bands ($\langle G(\nu)^2 \rangle = 2.861$) and of the three SPT bands ($\langle G(\nu)^2 \rangle = 1.107$). Note that in our analysis we are neglecting the less important KSZ component of the WHIM. Apart from being fainter, this is justified because the TSZ and KSZ WHIM power spectra have very similar shapes, rendering a joint fit of both components very degenerate.

We computed MCMCs in three different cases: to reproduce the analysis of Keisler et al. (2011) one run contained only the clusters SZ contribution; two other runs included both cluster and TSZ WHIM contributions, each with a fixed value of the IGM temperature, $T_{\text{IGM}} = 10^{3.6}$ and $10^{4.0}$ K. For each of these three cases, we ran eight independent chains with a total number of $\sim 350,000$ samples. The Gelman & Rubin (1992) criterion showed that all our chains had converged; in all cases the R statistic was well below 1.2. For instance, $R \approx 1.01$ for A_{WHIM} and ≈ 1.003 for the other parameters, when the WHIM component was included, and $R \approx 1.001$ when it was not. Keisler et al. (2011) used a Gaussian prior in the SZ cluster amplitude, $A_{\text{CL}} = 5.5 \pm 3.0 \mu\text{K}^2$, derived by Shirokoff et al. (2011) from an analysis of an earlier SPT data release. To determine the bias introduced by this prior on the WHIM amplitude, we ran our MCMCs with and without prior. No significant differences were found (except, of course, on the best-fit value of A_{CL} itself) and henceforth we will quote results with no prior.

4 RESULTS AND DISCUSSION

In Fig. 3 we represent the marginalized likelihood functions of the amplitude of the TSZ anisotropy generated by WHIM (Fig. 3a), TSZ and KSZ anisotropy generated by clusters (Fig. 3b), physical baryon density (Fig. 3c) and of the amplitude of matter density perturbations at $8h^{-1}\text{Mpc}$ (Fig. 3d). For an easier comparison, all likelihoods were normalized to unity. As mentioned above, the results presented do not include a prior on A_{CL} . Blue and red lines correspond to $T_{\text{IGM}} = 10^{3.6}$ and $10^{4.0}$ K, while the cyan lines correspond the results when no WHIM is included. Adding a WHIM component marginally decreases A_{CL} and σ_8 . In Fig. 4 we plot the two-dimensional likelihoods for different pairs of parameters. The figure shows that A_{WHIM} is degenerate with respect to other parameters, especially with respect to A_{CL} and σ_8 , and that it remains compatible with zero at the $2\text{-}\sigma$ level. The $1\text{-}\sigma$ contours of the $A_{\text{WHIM}} - \sigma_8$ plot appear slightly curved downwards for increasing A_{WHIM} , reflecting the (marginal) decrement of σ_8 when we include the WHIM TSZ anisotropy. Finally, the right panel shows how $\Omega_B h^2$ decreases when there is no WHIM contribution while A_{CL} remains almost unaffected. The dashed lines show the contours when no WHIM anisotropy is included.

In Fig. 5 we compare the measured WMAP 7yr (red filled circles) and SPT (blue filled circles) with our best-fit models in two cases (a) with a WHIM anisotropy with $T_{\text{IGM}} = 10^{3.6}$ K and (b) without a WHIM component, represented by (indiscernible) solid lines. We also plot the different components: primordial CMB (dashed lines), TSZ from WHIM (dotted line), SZ from galaxy clusters (dashed-dotted lines) and emission from point sources (both Poisson and clustered terms; dashed-triple-dotted lines). For visual purposes, we have scaled the WHIM component to the WMAP frequencies and the cluster component to the SPT frequencies.

Table 1 shows the parameters that define our best-fit cosmological model for our three MCMC (without A_{CL} prior). These parameters are derived from the median of the marginalized posterior probability density function, and their confidence intervals encompass the 68% of the probability around those points. The parameters derived when no WHIM component is included differ by less than 2% from those of Keisler et al. (2011). In the three cases considered by us, the amplitude of the SZ signal from clusters or from the WHIM is compatible with zero at the 2σ level. From the marginalized likelihood distributions we derive upper limits, at the 95.4% C.L., of $A_{\text{WHIM}} < 43.6 \mu\text{K}^2$ and $< 42.7 \mu\text{K}^2$, for $T_{\text{IGM}} = 10^{3.6}$ K and $10^{4.0}$ K, respectively. Taking the most-likely A_{WHIM} at face value, from the measured values of $\Omega_B h^2$, H_0 and σ_8 given in the table, we can determine the value of α that reproduces the amplitude of A_{WHIM} for each value of T_{IGM} . By interpolating in our grid of models we find $\alpha = 2.46, 3.40$ for $T_{\text{IGM}} = 10^{3.6}, 10^{4.0}$ K, respectively.

For each of these values of α we can compute the baryon content residing in the WHIM filaments with overdensities in the range $[\xi_1, \xi_2]$. To this aim, we use the formalism de-

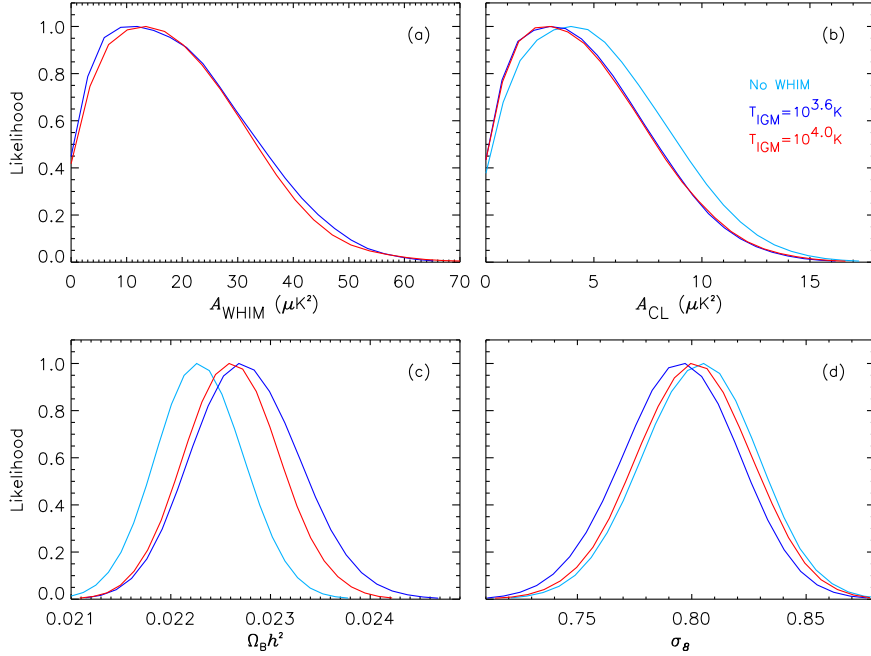


Figure 3. Marginalized likelihoods for the WHIM TSZ amplitude at $\ell = 300$ (A_{WHIM}), for the combined TSZ+KSZ amplitude at $\ell = 3000$ from galaxy clusters (A_{CL}), for the physical baryon density ($\Omega_{\text{B}}h^2$), and for the amplitude of matter density fluctuations in scales of $8 h^{-1}$ Mpc (σ_8). We plot our results for the two IGM temperatures, $T_{\text{IGM}} = 10^{3.6}$ K (blue) and $10^{4.0}$ K (red), as well as when no WHIM signal is introduced (cyan).

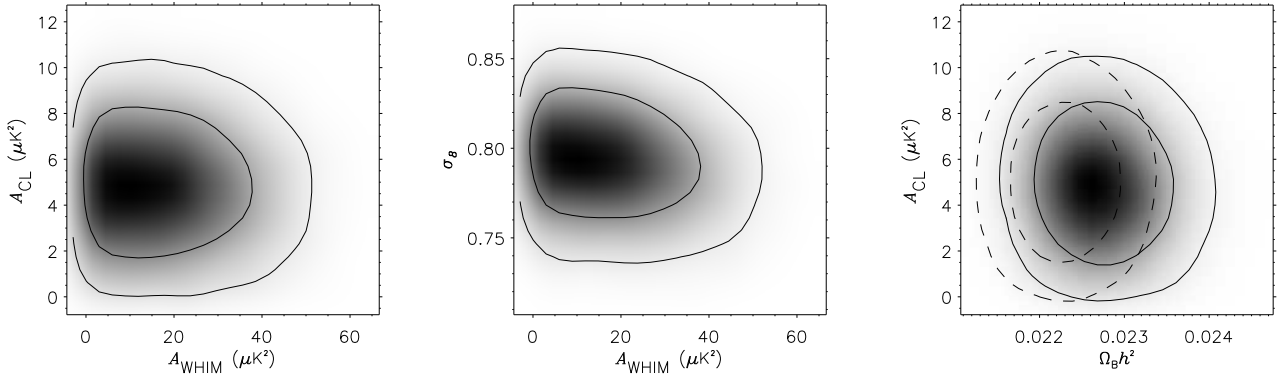


Figure 4. Mean two-dimensional likelihoods for three combination of parameters, for $T_{\text{IGM}} = 10^{3.6}$ K. Solid lines represent the 1σ and 2σ confidence regions. Dashed lines in the right panel correspond to the case with no WHIM component.

scribed in Suarez-Velázquez et al. (2013b). The mass fraction is given by $M(\xi_1, \xi_2) = \bar{\xi}^{-1} \int_{\xi_1}^{\xi_2} \xi F(\xi)$, where $\bar{\xi}$ is the mean of the distribution and $F(\xi)$ is the log-normal probability distribution function. The integration range must be limited to those overdensities where the non-linear evolution is well described by our model. As a criteria, we took $\xi_2 \leq 100$ and $\xi_1 = \xi_{\text{median}} + \sigma$, with σ the standard deviation of the log-normal distribution. To include only scales that

undergo shock heating we also require as necessary condition that $\xi_1 > 2$ at all redshifts. Since ξ_1 and T_{IGM} are redshift dependent, the fraction of baryons residing in the WHIM filaments is a decreasing function of z . For $\alpha = 2.46, 3.40$ and $T_{\text{IGM}} = 10^{3.6}, 10^{4.0}$ K the derived baryon fractions at $z = 0$ are respectively $\Omega_{\text{B,WHIM}}/\Omega_{\text{B}} \approx 0.43$ and 0.47 . Notice that even if the value of α is rather uncertain, the baryon fraction varies little within the allowed parameter space. Our

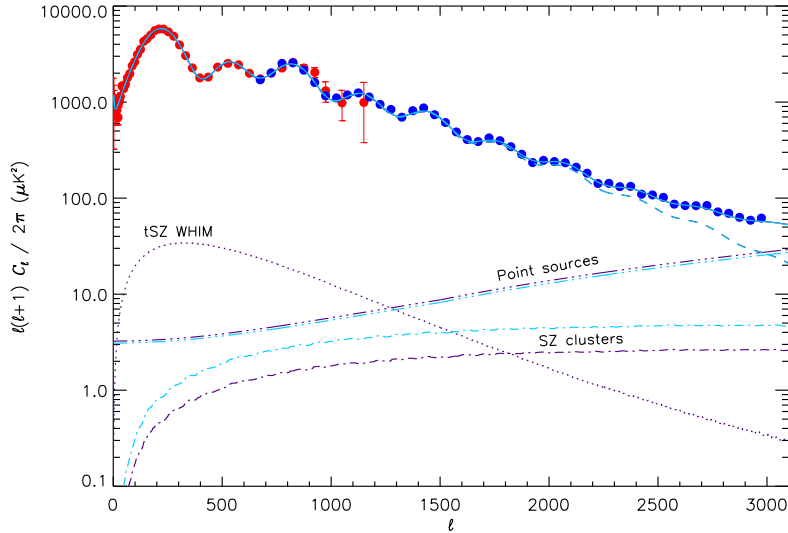


Figure 5. Experimental power spectra measured by WMAP7 (red dots) and SPT (blue dots) compared with our fitted models. Dashed, dotted, dashed-dotted and dashed-triple-dotted lines correspond respectively to the primordial CMB, WHIM tSZ, combined tSZ and kSZ signals from clusters, and point sources (combing the terms coming from Poisson and clustered distributed sources). Solid lines represent the sum of all these components. We compare our results including the WHIM TSZ component (magenta curves) with the case when no WHIM component is included (cyan curves). This plot corresponds to the case of $T_{\text{IGM}} = 10^{3.6}$ K, and shows no significant differences with respect to the case of $T_{\text{IGM}} = 10^{4.0}$ K.

result is slightly above the 0.29 ± 0.13 fraction of baryons that remain unidentified according to Shull et al. (2012). The baryons detected through TSZ anisotropies will include baryons on low dense regions identified by other techniques, like some of the OVI absorption systems; after correcting the double accounting, the fraction of identified baryons would be close to unity.

In our chains we have fixed T_{IGM} ; then, including the WHIM contribution adds only one parameter, A_{WHIM} (that is related with α), to the chain. The improvement in the quality of the fit is minimal: in the best case $\Delta\chi^2 \simeq -0.4$. Therefore the data fails to provide any significant evidence of the existence of the WHIM. Not unexpectedly, when including a WHIM anisotropy, A_{CL} decreases by 10%, enhancing the disagreement between the measured cluster SZ anisotropies and the theoretical expectation. However, the discrepancy is alleviated since σ_8 also decreases. In the model with $T_{\text{IGM}} = 10^{3.6}$ K, the lower value of σ_8 reduces the theoretical SZ signal by 7% compensating the lower value of A_{CL} found. To make the cluster SZ signal compatible with the theoretical predictions we would need $\sigma_8 \approx 0.73$, much smaller than the measured value.

The results of Table 1 can be understood taking into account the difference in the angular scales probed by WMAP and SPT. The information on the radiation power spectrum provided by these instruments is complementary with each other. In WMAP, at low ℓ 's errors are dominated by sampling variance and at high ℓ 's by noise. By contrast, the radiation spectrum has been best measured by the SPT

in the range $\ell \simeq 600 - 3000$. Then, while WMAP data is mostly sensitive to the range where the WHIM contribution is largest, around the first and second acoustic peaks, SPT data constrain better the cluster TSZ contribution. The first acoustic peak occurs at $\ell \simeq 200$, its amplitude is $\ell(\ell+1)C_\ell/2\pi \simeq 6000 \mu\text{K}^2$ and scales approximately as σ_8^2 . In ΛCDM if all parameters are held fixed but σ_8 decreases by 0.5%, the amplitude of the first acoustic peak decreases by $\sim 1\%$. i.e., there could be a WHIM as high as $60 \mu\text{K}^2$ at the maximum. Since WMAP operates at Rayleigh-Jeans frequencies, this corresponds to an amplitude $A_{\text{WHIM}} = 15 - 20 \mu\text{K}^2$, compatible with the results of Fig. 3. Even though the WHIM contribution falls for $\ell \geq 1000$, the tail of the distribution overlaps with cluster anisotropies and the SPT data would suppress the latter (see Fig. 5).

Since our results are compatible with zero WHIM contribution, one could interpret them as an indication (1) that the data has not enough statistical power to identify the WHIM contribution or (2) that the WHIM is not a strong contributor to the baryon budget. While the estimated values of the total baryon mass fraction in groups and clusters are still lower than the latest CMB measurement of the same quantity (Giodini et al. 2009), it seems implausible that a better modelling of the gas physics could eventually solve the WHIM problem. If clusters and groups store more baryons than presently believed, the discrepancy between the SZ amplitude of clusters measured by SPT and WMAP with the numerical expectations summarized in Komatsu et al (2011)

Parameter	No WHIM	WHIM $T_{\text{IGM}} = 10^{3.6}$ K	WHIM $T_{\text{IGM}} = 10^{4.0}$ K
$\Omega_{\text{B}}h^2$	0.0223 ± 0.0004	0.0228 ± 0.0005	0.0226 ± 0.0005
$\Omega_{\text{CDM}}h^2$	0.110 ± 0.005	0.111 ± 0.005	0.111 ± 0.005
100θ	1.041 ± 0.002	1.042 ± 0.002	1.042 ± 0.002
τ	$0.0857^{+0.0063}_{-0.0070}$	$0.0864^{+0.0064}_{-0.0072}$	$0.0865^{+0.0064}_{-0.0071}$
n_{S}	0.964 ± 0.011	0.962 ± 0.011	0.967 ± 0.011
$\ln(10^{10} A_{\text{S}})$	3.19 ± 0.04	3.18 ± 0.04	3.17 ± 0.04
Y_{He}	0.2478 ± 0.0002	0.2480 ± 0.0002	0.2479 ± 0.0002
A_{WHIM}		$19.36^{+13.37}_{-13.34}$	$19.16^{+12.65}_{-12.91}$
A_{CL}	$5.15^{+3.34}_{-3.37}$	$4.58^{+3.11}_{-3.14}$	$4.60^{+3.12}_{-3.14}$
$A_{\text{PS}}^{\text{Poisson}}$	$20.40^{+2.93}_{-2.92}$	20.23 ± 2.89	$20.32^{+2.89}_{-2.87}$
$A_{\text{PS}}^{\text{Clustered}}$	$5.11^{+2.22}_{-2.28}$	$5.03^{+2.21}_{-2.25}$	$5.05^{+2.20}_{-2.26}$
σ_8	0.803 ± 0.024	0.795 ± 0.025	0.800 ± 0.024
Ω_{Λ}	0.735 ± 0.025	0.738 ± 0.025	0.736 ± 0.025
Ω_{M}	0.265 ± 0.025	0.262 ± 0.025	0.264 ± 0.025
z_{re}	$10.40^{+1.17}_{-1.16}$	10.33 ± 1.18	$10.39^{+1.18}_{-1.17}$
H_0	$71.00^{+2.13}_{-2.14}$	$71.53^{+2.19}_{-2.20}$	71.27 ± 2.14
χ^2	3756.04	3755.84	3755.66

Table 1. Concordance Λ CDM best fit parameters for each MCMC. We show the results for the three cases that we have considered: no WHIM, and a WHIM component with T_{IGM} temperatures of $10^{3.6}$ and $10^{4.0}$ K, respectively. Parameters are derived from the median of the marginalized posterior probability density functions, while the confidence intervals are calculated from the 68% area around those points. The last row shows the χ^2 of these models. The amplitudes A_{WHIM} , A_{CL} , $A_{\text{PS}}^{\text{Poisson}}$, $A_{\text{PS}}^{\text{Clustered}}$ are given in units of μK^2 and the Hubble constant H_0 in $\text{kms}^{-1}\text{Mpc}^{-1}$.

would be even more acute. What our results indicate is the difficulty to accommodate a WHIM component that brings the measured cluster TSZ signal in agreement with the theoretical predictions. The reason of this discrepancy might not be the measured value of σ_8 or A_{SZ} , but the lack of understanding of some of the aspects of the cluster physics that are introduced in the simulations.

5 CONCLUSIONS.

We have explored the parameter space of the concordance Λ CDM model using two SZ contributions: one due to the combined KSZ and TSZ effects from the unresolved cluster population, the other due to the TSZ from WHIM. We have fitted this model to the combined WMAP 7yr and SPT data, at present the best data-set publicly available, covering the multipole range $\ell = [2, 3000]$. We have found that a WHIM component with an amplitude of $\sim 20 \mu K^2$ at $\ell \sim 300$ is compatible with the data. This new WHIM component results in a 10% decrement in the amplitude of the SZ signal ascribed to galaxy clusters, while the cosmological parameters do not change significantly; $\Omega_{\text{B}}h^2$ is 2% higher, and σ_8

decreases by 1%. This new fit does not solve the discrepancy between the measured amplitude of the cluster power spectrum and the theoretical expectation; this would require a considerably lower value of σ_8 . However, since σ_8 is tightly constrained by the data, this could be an indication of improper modelling of cluster evolution, gas dynamics, and of the resulting pressure profiles, both theoretically and numerically. Our analysis shows that a WHIM contribution is compatible with WMAP and SPT data and, if this contribution is well described by our model, the average properties of the WHIM can be measured. Since the cosmological parameters (σ_8 , Ω_{B} and h) are determined from the CMB anisotropy data, measuring the WHIM contribution allows to constrain the other two parameters, namely, the cut-off length of the baryons power spectrum, parametrized by T_{IGM} , and the phase diagram parameter α that also determine the amplitude of the WHIM anisotropy. For $A_{\text{WHIM}} \sim 20 \mu K^2$ the Kang et al. (2005) phase diagram parameter is constrained to be in the interval $\alpha \simeq [2.5, 3.4]$, consistent with the estimates derived from simulations. The fraction of baryons that would reside in this phase, between 43% and 47%, would be large enough to close the baryon census problem summa-

rized in Shull et al. (2012). These are the first constraints on the physical state and abundance of the WHIM presented to date.

Planck, with its wide coverage of frequencies and angular scales, could help to unambiguously measure this WHIM component, separating it from the cluster contribution, and to set more stringent constraints on the WHIM physical properties. The power spectrum amplitude scales as $C_\ell^{\text{WHIM}} \propto A_{\text{WHIM}} G(\nu)^2$. If $A_{\text{WHIM}} = 10 - 15 \mu\text{K}^2$ at Planck frequencies it will change from zero at 217 GHz to $\sim 60 \mu\text{K}^2$ at 40 GHz (decrement) and 353 GHz (increment). This represents a 2% variation across the observed range. If foreground contributions, that also change with frequency, are subtracted down to this level, then the variation of the power spectrum will be an indication of the WHIM TSZ contribution.

ACKNOWLEDGMENTS

RGS acknowledges support from the Cosolider Ingenio programme of the Spanish Ministerio de Economía y Competitividad (project “Exploring the Physics of Inflation”). ISV thanks the DAAD for the financial support, grant A/08/73458. FAB acknowledges financial support from the Spanish Ministerio de Economía y Competitividad (grants FIS2009-07238, FIS2012-30926 and CSD 2007-00050). He also thanks the hospitality of the Leibniz Institute für Astrophysik.

REFERENCES

- Atrio-Barandela, F., Kashlinsky, A., Kocevski, D., & Ebeling, H. 2008, *ApJ*, 675, L57
- Atrio-Barandela, F., & Mücke, J. P. 1999, *ApJ*, 515, 465
- Atrio-Barandela, F., & Mücke, J. P. 2006, *ApJ*, 643, 1
- Atrio-Barandela, F., Mücke, J. P., & Génova-Santos, R., 2008, *ApJ*, 674, L61
- Birkinshaw, M. 1999, *Phys. Rep.*, 310, 97
- Cappelluti, N., et al. 2012, *MNRAS*, 247, 651
- Cen, R., & Ostriker, J.P. 1999, *ApJ*, 519, L109
- Cen, R., & Ostriker, J.P. 2006, *ApJ*, 650, 560
- Choudhury, T.R., Padmanabhan, T., & Srianad, R., 2001, *MNRAS*, 322, 561
- Coles, P., & Jones, B. J. T. 1991, *MNRAS*, 248, 1
- Davé, R., et al. 2001, *ApJ*, 552, 473
- Fukugita, M., & Peebles, P.J.E. 2004, *ApJ*, 616, 643
- Gelman, A. & Rubin, D. 1992, *Stat. Sci.*, 7, 457
- Génova-Santos, R., Rubiño-Martín, J. A., Rebolo, R., et al. 2008, *MNRAS*, 391, 1127
- Génova-Santos, R., Atrio-Barandela, F., Mücke, J. P., & Klar, J.S., 2009, *ApJ*, 700, 447
- Giodini, S., et al. 2009, *ApJ*, 703, 982
- Hand, N., Addison, G. E., Aubourg, E., et al. 2012, *Physical Review Letters*, 109, 041101
- Hernández-Monteagudo, C., Génova-Santos, R. & Atrio-Barandela, F. 2004, *ApJ*, 613, L89
- Kang, H. et al. 2005, *ApJ*, 620, 21
- Kaastra, J. S., Werner, N., Herder, J. W. A. d., et al. 2006, *ApJ*, 652, 189
- Kashlinsky, A., Atrio-Barandela, F., Kocevski, D., & Ebeling, H. 2008, *ApJ*, 686, L49
- Kashlinsky, A., Atrio-Barandela, F., Ebeling, H., Edge, A., & Kocevski, D. 2010, *ApJ*, 712, L81
- Keisler, R. et al (2011) *ApJ*, 743, 28.
- Kitaura, F. S., Jasche, J., Li, C., et al. 2009, *MNRAS*, 400, 183
- Komatsu, E. et al. 2011, *ApJSS*, 192, 18
- Komatsu, E. & Kitayama, T. 1999, *ApJ*, 526, L1
- Larson, D., Dunkley, J., Hinshaw, G., et al. 2011, *ApJS*, 192, 16
- Lewis, A., Challinor, A., & Lasenby, A. 2000, *ApJ*, 538, 473
- Lewis, A., & Bridle, S. 2002, *Phys.Rev.D*, 66, 103511
- Nicastro, F., Mathur, S., Elvis, M., et al. 2005, *ApJ*, 629, 700
- Padilla-Torres, C.P. et al. 2009, *MNRAS*, 396, 53
- Planck Collaboration, Ade, P. A. R., Aghanim, N., et al. 2011, *A&A*, 536, A8
- Planck Collaboration 2012. *Planck Intermediate Results VIII*, 2012, *A&A*, 550, 131
- Roncarelli, M., et al. 2012, *MNRAS*, 424, 1012
- Shirokoff, E. et al. 2011, *ApJ*, 736, 61
- Shull, J. M., Smith, B. D., & Danforth, C. W. 2012, *ApJ*, 759, 23
- Smith, B. D., Hallman, E., Shull, J. M., & OShea, B. 2011, *ApJ*, 731, 6
- Suarez-Velásquez, I. F., Kitaura, F. S., Atrio-Barandela, F., & Mücke, J. P. 2013a, *ApJ*, submitted
- Suarez-Velásquez, I. F., Mücke, J. P., & Atrio-Barandela, F. 2013b, *MNRAS*, accepted
- Sunyaev, R. A., & Zel’dovich, Y. B. 1970, *ApSS*, 7, 3
- Sunyaev, R. A., & Zel’dovich, Y. B. 1972, *CoASP*, 4, 173
- Theuns T., Schaye J., Zaroubi S., Kim T.-S., Tzanavaris P., Carswell B., 2002, *ApJ*, 567, L103
- Tittley E. & Meiksin A. 2007, *MNRAS*, 380, 1369
- Yao, Y., Shull, J. M., Wang, Q. D. & Cash, W. 2012, *ApJ*, 746, 166

This paper has been typeset from a \TeX / \LaTeX file prepared by the author.